Nanotechnology **10** (1999) 166–173. Printed in the UK PII: S0957-4484(99)97404-4

Observation of switching in a quantum-dot cellular automata cell

Gary H Bernstein†, Islamshah Amlani, Alexei O Orlov, Craig S Lent and Gregory L Snider

Department of Electrical Engineering, University of Notre Dame, Notre Dame, IN 46556, USA

Received 3 September 1998

Abstract. The notion of quantum-dot cellular automata (QCA) as a possible replacement paradigm for conventional transistor-based logic is reviewed. Experiments using metal tunnel structures demonstrating a functional QCA cell are presented. It is shown that single electron tunnelling transistors used as electrometers verify proper switching of the QCA cell. Additionally, we provide evidence for a QCA cell switching frequency of 14 MHz, and a calculated upper limit of more than 5 GHz.

1. Introduction

Although originally proposed in 1965, Moore's law [1] regarding exponential growth of IC density is still basically intact as we approach the year 2000. The advent of such technologies as copper interconnects [2], low-k dielectrics [3], and advanced optical [4] or other [5] lithography techniques promise a continuation for several more years. However, fundamental constraints of power dissipation, high electric fields in the drain and gate, and interconnect delays will in the not-too-distant future cause a slowing of the predicted growth.

It is prudent, then, to search for a replacement paradigm for computing which does not rely on power hungry transistors and relatively slow metal interconnects. The computational paradigm known as quantum-dot cellular automata (QCA) [6–10] is one such possibility. Computation with QCA follows the well-understood rules of Boolean logic, but relies on polarization of cells instead of voltages and currents to encode binary data. QCA offers many advantages over conventional technology including compatibility with nanostructures, simplified interconnects, and the possibility for extremes in density, power dissipation, and computational speeds.

The concept of QCA does not rely on any particular technology; possible ones include quantum dots in semiconductors [11], metal tunnel junctions [12–15], self-assembled dots [16] and, ultimately, molecules [8]. As the size of the dots decreases, charging energy and operating temperatures will increase. Therefore, a viable technology will consist of sufficiently small features that can be arranged practically into appropriate patterns over large areas, such as self-aligned structures or molecules. In this work we exploit the metal/tunnel junction system, as it is straightforward to fabricate and robust enough at low temperatures to allow demonstration of the basic principles.

† E-mail address: bernstein.1@nd.edu

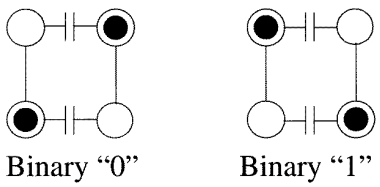

Figure 1. Ground states of the basic four-dot QCA cell [8].

One embodiment of the basic QCA cell is shown in figure 1. It consists of four dots separated vertically by tunnel barriers and horizontally by coupling capacitors [10]. If the system is charged with one extra electron per side, then the electrons will reside in opposite corners due to electrostatic repulsion. The energies of the two possible configurations are degenerate, but they can be used to encode both Boolean logic values '1' and '0'. It has been shown [8] that strings of cells arranged in a variety of ways can be used to implement wires and logic gates, including NOT, AND, OR, and majority gates. Figure 2 [9] shows a single-bit full adder composed entirely of QCA cells. For a dot size of 10 nm, it requires an area of less than 1.5 μm^2 and replaces about 30 transistors. For this and other QCA systems, data are both provided and detected at the edges, and no power is supplied directly to the interior of the array. Using a technique called 'adiabatic switching' [8], the signal propagates through sections of the array in a controlled, clocked manner by raising and lowering barriers and allowing sequences of cells to stabilize.

The experiments described here consist of a total of six dots, forming a four-dot QCA cell and two single electron transistor (SET) electrometers used as probes of dot occupancy (described below). A representation of the six-dot system is shown in figure 3(*a*), its schematic diagram including all independent sources is shown in figure 3(*b*), and a scanning electron micrograph is shown in figure 3(*c*). In figure 3(*b*), the input dots are labelled D_1 and D_2, and the output dots are labelled D_3 and D_4. E_1 and E_2 are SETs used

0957-4484/99/020166+08$19.50

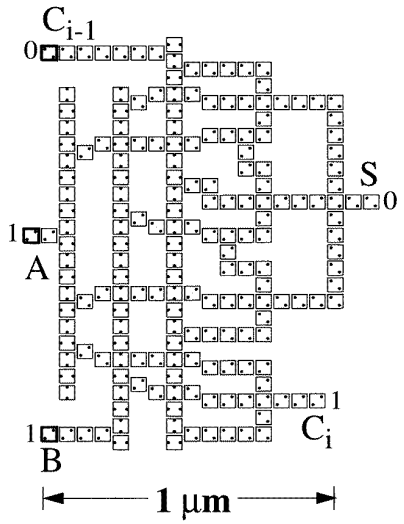

Figure 2. Single-bit, full adder composed entirely of QCA cells. Included in this system are such components as wires, inverters, and higher-level logic functions such as majority gates. Data are input on the left edge of the system and output on the right edge. No power is supplied to the interior of the array [9].

as electrometers, as first investigated by Lafarge *et al* [17]. The operation of the system will be discussed below.

The system is fabricated using three optical lithography steps followed by the metal/tunnel junction technique pioneered by Fultan and Dolan [18]. In this technique a double-layer of resist is exposed by electron beam lithography and developed, followed by angled evaporation, oxidation, and a final angled evaporation to create tunnel junctions. In our figure, the functional 'dots' or 'islands' consist of all metal that is isolated by tunnel junctions and connected to segments labelled as D_1 to D_4. Tunnel junctions are circled.

In this paper we first demonstrate the operation of a four-dot QCA cell. The sequence of switching operations is as follows: The gates labelled V_A and V_B representing input signals are scanned, a single electron switches position between input dots D_1 and D_2, and in response to this stimulus, an electron on the output dots D_3 and D_4 switches positions in the opposite directions as confirmed by the external probes. Secondly, we offer evidence of an experimentally determined minimum cell switching speed of 14 MHz with a theoretical upper limit greater than 5 GHz for the existing device.

2. Detection schemes

One obvious problem in the development of QCA technology is the manner of detecting the internal behaviour of cells accurately without disturbing their operation. In this paper we utilize two distinct techniques for accomplishing this. The first technique, described schematically in the input dots of figure 3(*a*), relies on the conductance of two series-coupled dots ('double-dots') as a function of all possible gate voltages to determine the relative change in dot populations. The second technique for determining dot population, shown on the right in figure 3(*a*), is the use of single electron transistors as electrometers in close proximity to the dots.

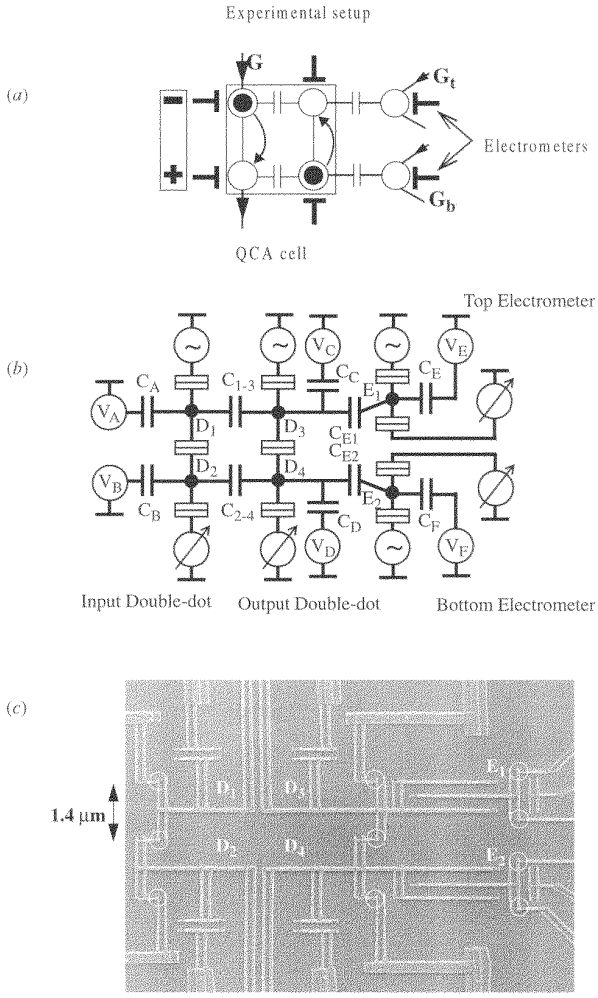

Figure 3. Representations of the metal tunnel junction system studied in this work. (*a*) Experimental configuration of double-dots and associated single-dot electrometers, (*b*) schematic diagram of six-dot QCA system, and (*c*) scanning electron micrograph of metal system on SiO_2 on Si. The functional metal 'dots' or 'islands' consist of all of the metal isolated by tunnel junctions and connected to segments labelled as D_1 to D_4. Tunnel junctions are circled.

We discuss first the use of series conductance for determining the relative electron population of the dots. Figure 4(*a*) is a surface plot of the conductance of the series double-dot at a dilution refrigerator temperature of 10 mK and magnetic field of 1 T (to suppress superconductivity effects). Each peak in conductance, occurring at 'triple points,' is a point of instability in the dot population at which charge transfer between the dots is favourable. Figure 4(*b*) depicts the same information in the form of a contour map. This charging diagram has a characteristic 'honeycomb' structure with each cell representing a stable charge configuration [19]. Here we arbitrarily assign one cell to be the unpopulated state of the double-dot, i.e. the population is assigned as $(n_{\mathrm{top}} = 0, n_{\mathrm{bot}} = 0)$ where n_{top} is the excess electron population of the top dot and n_{bot} is that of the bottom dot.

By traversing certain paths through the gate voltage space, the population of the dots can be changed very accurately. Deviating from a bias point in a particular direction on this map can result in stable and well-

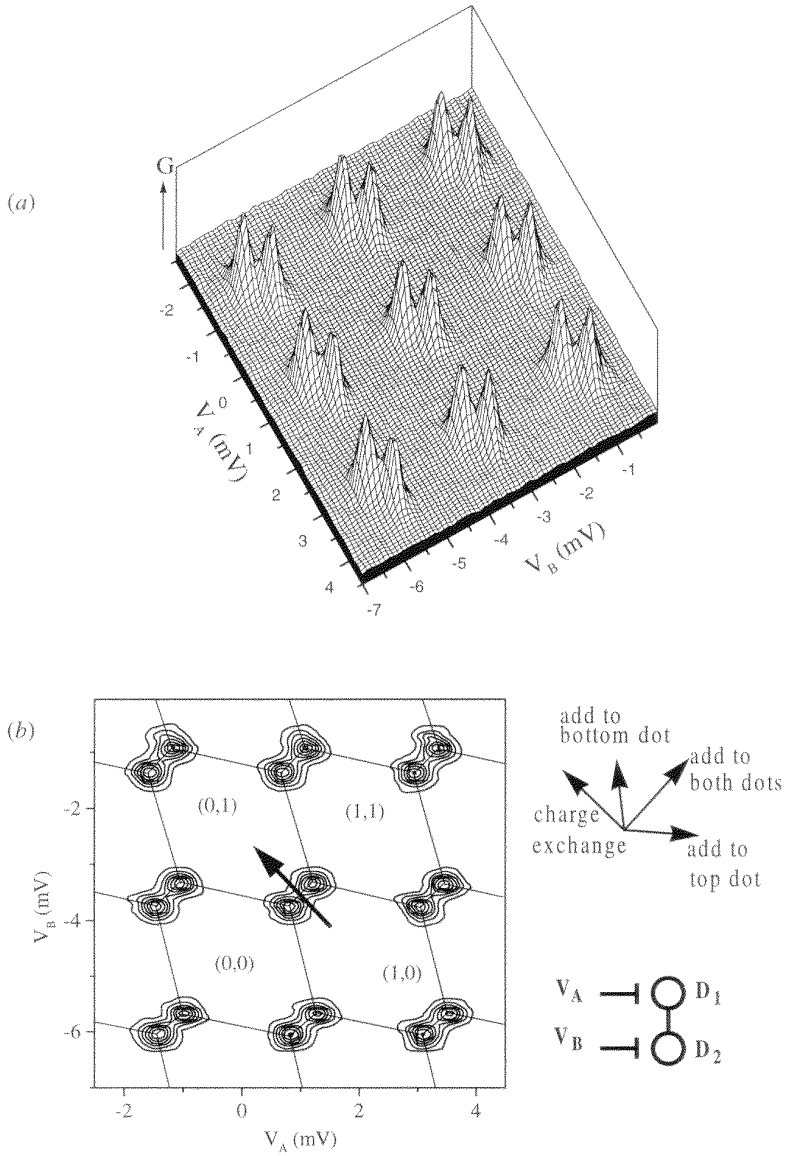

Figure 4. Charging diagram showing conductance of series double-dot as a function of both gate voltages plotted as (*a*) surface plot and (*b*) contour plot. Shown in (*b*) is a schematic diagram of the subsystem measured for this figure. It can be seen in (*b*) that the regions of dot population map out a honeycomb shape, where each cell is a region of stable dot occupancy in which conductance is effectively zero. Total excess electron dot population cannot be known exactly, but relative values can be determined. Here we have arbitrarily assigned one cell as having a population of the top and bottom dots to have occupancy of (top, bottom) = (0, 0) electrons. An electron is added or removed from each dot as its gate potential is varied. Indicated to the right of (*b*) are the changes in electron population for several directions. The portion of interest for QCA operation is the border between the (1, 0) and (0, 1) stable regions.

characterized dot occupancies. For example, increasing V_A (in this case the input dots are used) increases the population of the top dot but has little effect on that of the bottom dot. Note that in our experiments we utilize all of the cross capacitances of the system to adjust each gate voltage so as to minimize capacitive coupling between the gates on unrelated dots.

Of special interest is the path between cells labelled (1, 0) and (0, 1). These cells are the stable states of one extra electron on the top and bottom dot, respectively. We sweep the gate voltages in a 'push–pull' configuration, with a distance along the path of $V_{\mathrm{diag}} = (\Delta V_{g1}^2 - \Delta V_{g2}^2)^{1/2}$. As the gate voltages change so as to traverse a path along the arrow, the double-dot changes state from having a surplus electron on the top dot to one on the bottom dot. This is exactly the behaviour required of an operational QCA cell. We show below that by controlling the population of the input dot in this manner, this change in population causes the opposite effect in the output dot, demonstrating a complete, operational QCA cell.

Our second method of detecting the presence of electron charging in the dots is through the use of electrometers consisting of nearby SETs. Figure 5(*a*) shows the conductance of an SET versus gate voltage. Each peak in conductance represents a situation in which it is energetically favourable for an electron to overcome the electrostatic repulsion of electrons on the island. Once an additional electron is locked onto the island, the island potential,

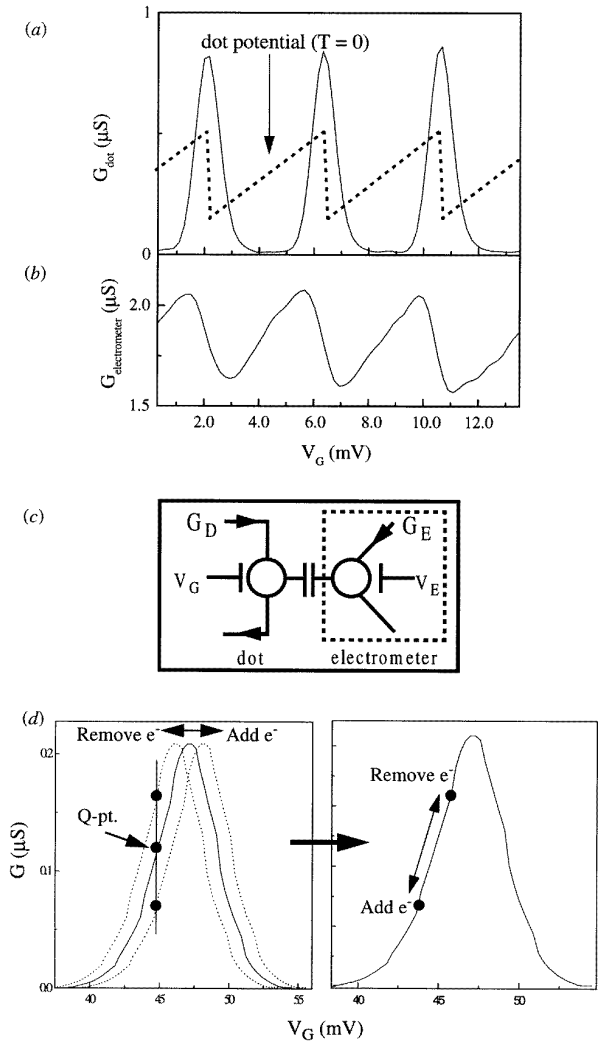

Figure 5. Operation of single electron transistor based electrometer. (*a*) Single-dot conductance as a function of gate voltage with a superimposed plot of its calculated ($T = 0$ K) potential, (*b*) measured dot potential from a coupled electrometer, (*c*) schematic representation of a single-dot with a coupled electrometer, and (*d*) a single conductance peak demonstrating a shift due to the addition or removal of an electron from a nearby dot. The experimental data in (*b*) are spread out compared to the potential in (*a*) due to a finite electron temperature of approximately 75 mK.

Φ, must be lowered further to allow in another electron. The potential necessary to effect a change in conductance need not necessarily come from the gate, but may come from any other surrounding source. Figure 5(*c*) is a schematic representation of a dot with a coupled electrometer. Figure 5(*d*) demonstrates the shift of a single conductance peak due to the addition or removal of an electron on a nearby dot. If the electrometer is biased at a Q-point, the nearby potential shift is superimposed on the gate voltage, causing conductance to decrease or increase, respectively, for biasing on the leading edge of the conductance peak. Biasing on a linear portion of the edge results in direct qualitative evaluation of the nearby dot potential, and using known, measured coupling capacitances, the potential and electron occupancy can be accurately determined. Figure 5(*a*)

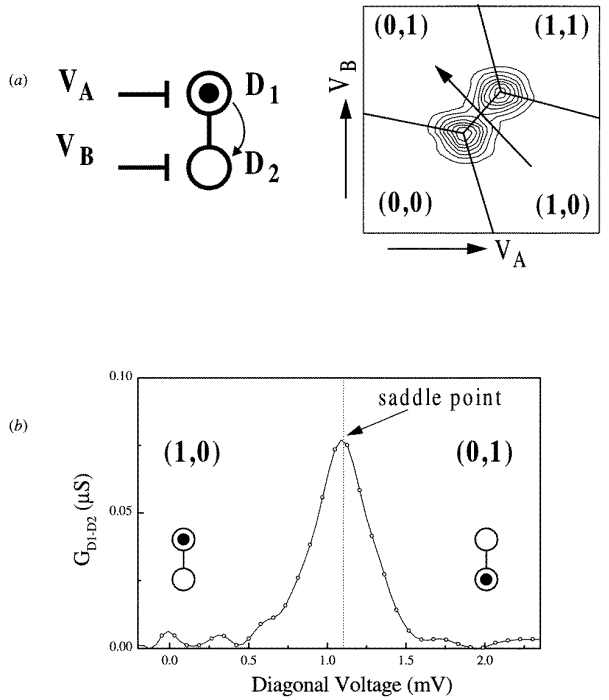

Figure 6. Switching behaviour of a QCA cell. (*a*) Schematic diagram of a subsystem measured for these data, and an enlarged view of the boundary between the (1, 0) and (0, 1) regions and (*b*) conductance of the double-dot along the switching path.

includes a theoretical plot of the dot potential (broken line) corresponding to peaks in dot conductance at $T = 0$ K. The potential increases slowly as the gate voltage is increased and drops sharply as an electron is added to the dot, cancelling the excess potential from the gate. The addition of an electron corresponds exactly to the dot instability where current flows through the dot. Figure 5(*b*) shows experimental data of electrometer conductance, at an electron temperature $T = 75$ mK, corresponding to the conductance of the dot under test. It can be seen that there is qualitative agreement between the electrometer conductance and the potential on the observed dot, demonstrating that changes in the occupancy of dots can be accurately known by use of electrometers.

3. QCA switching behaviour

Figure 6 demonstrates the switching behaviour of a QCA cell. Figure 6(*a*) is an enlarged view of the boundary between the (1, 0) and (0, 1) regions for the input dots D_1 and D_2. As V_A and V_B are swept on a path along the arrow, crossing the boundary is equivalent to an electron switching from the top dot to the bottom dot. Although the actual behaviour is for conductance to increase through the region of instability, and many electrons travel through the dots, the resulting dot population is equivalent to a switch in the position of one extra electron. Figure 6(*b*) shows the conductance of the double-dot along the switching path. At the boundary, a saddle point in conductance exists due to thermal broadening. At $T = 0$ K, the conductance peak would not exist, and conductance would occur only at the triple points. In this

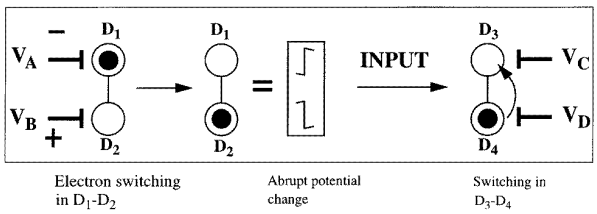

Figure 7. Switching process of a complete QCA cell.

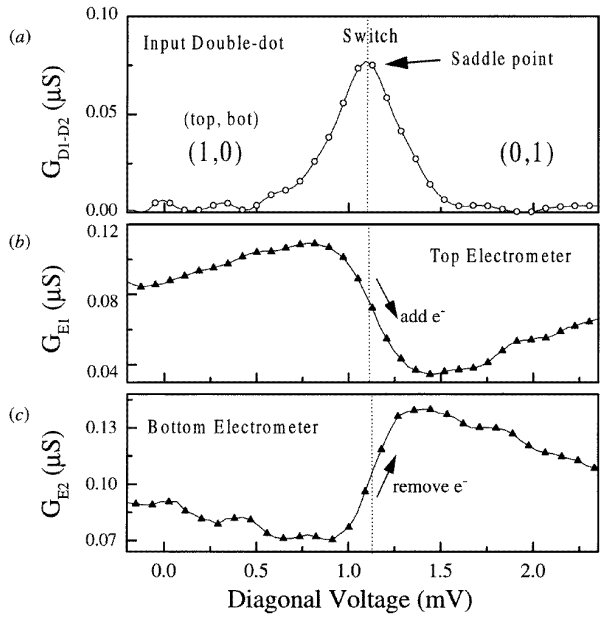

Figure 8. Experimental demonstration of switching in the QCA cell. (*a*) Conductance of the input double-dot showing saddle point at critical V_{diag} of an electron switch, (*b*) conductance of the top electrometer showing decrease as verification of addition of an electron, and (*c*) conductance of the bottom electrometer showing increase as verification of loss of an electron.

work we use the conductance at the saddle point as an effective means of determining the boundary between the (1, 0) and (0, 1) regions.

As an electron is effectively switched from the upper to the lower dot, the resulting potential difference plays a major role in the switching process. Figure 7 is a deconstruction of figure 3(*a*) in which each step of the process is broken out, illustrating the switching process of a complete QCA cell. As an electron switches from D_1 to D_2, the potential on D1 increases (loses an electron) and that on D_2 decreases (gains an electron). The output double-dot, biased at the boundary between the (1, 0) and (0, 1) regions on its charging diagram, senses the changes in its neighbouring potentials, which are sufficient to switch an electron at the output from D_4 to D_3.

Experimental data confirming this operation are given in figure 8. The charging diagrams for the input and output dots are determined independently, and the input double-dot is biased near the peak of the saddle point conductance at the boundary of the (0, 1) and (1, 0) regions, as shown in figure 8(*a*). As the border between (1, 0) and (0, 1) states is crossed, the electron switches from D_1 to D_2. In response, an electron switches from D_4 to D_3, as verified by direct observation of the electrometers, shown for both the top (figure 8(*b*)) and bottom (figure 8(*c*)) dots. As discussed above, for biasing on the rising edge of the electrometer conductance peak, a decrease in conductance of electrometer E_1 signifies a decrease in potential and therefore the addition of an electron onto D_3, which is consistent with figure 8(*b*). Likewise, an increase in electrometer E_2 conductance signifies the loss of an electron from D_4, which is consistent with figure 8(*c*).

Support for our conclusions is provided in figure 9, showing the theoretical and experimental curves of the potential change on D_3 as a function of the diagonal voltage on D_1–D_2. In figure 9(*a*), the experimental curve of the potential on D_3 is computed from the conductance of E_1, and the theoretical curve is obtained by minimizing the total electrostatic energy of the whole system. We measure all dot capacitances and use them to calculate the minimum classical electrostatic energy for all six dots and associated metallization. Minimum energy charge configurations are calculated for each setting of the input diagonal voltage, given the condition that the charge on each dot of the QCA cell be an integer multiple of electronic charge, *e*. The effect of finite temperature on the potential and the charge is simulated by thermodynamic averaging over all accessible charge configurations. We have achieved very good agreement between theory and experiment using only substrate background charge and temperature as fitting parameters. The background charge serves only to shift the diagonal voltage but otherwise has no effect on the curves. The best fit to experiment is obtained for 75 mK, which is in close agreement with the actual device temperature, as determined by peak-shape analysis [20]. Although the base temperature of our refrigerator is 10 mK, it is reasonable that some heating of the device occurs through the leads and from the finite applied potentials (typically 4 μV between source and drain) used in the measurements.

Calculations shown in figure 9(*b*) show that the input double-dot is 100% polarized during switching, i.e. the electronic charge resides totally on one dot for biasing on either side of the cell boundary. Figure 9(*c*) confirms the reverse change in polarization for the output dots as the polarization of the input dots switches. We calculate a 70% change in polarization of the output double-dot. This can be increased by designing larger coupling capacitors, C_{1-3} and C_{2-4}.

Further evidence that the electrometers are responding to a switch in occupation of the output dots and not merely the input gate voltages is as follows.

(1) If the output dots switched in response to the input gate voltages only, the electrometer conductance shifts (a) would not occur precisely at the saddle point conductance of the input double-dot where the dot populations of the input dots switch, (b) would not switch in unison, and (c) would switch in the opposite directions from those observed.

(2) If the electrometer conductances were affected only by the input gate voltages, they would rise or fall monotonically and not show sharp switching behaviour. Therefore, we conclude that the switching behaviour measured here shows actual QCA behaviour and demonstrates that it may be feasible to operate larger arrays of QCA cells.

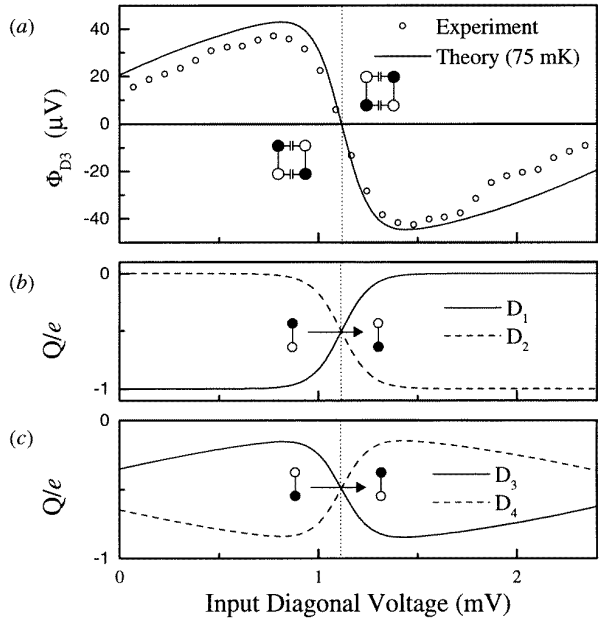

Figure 9. (*a*) Experimental and theoretical curves showing the potential change on dot D_3 as a function of the input diagonal voltage. The simulation results at 75 mK (full curve) closely match the experimental data (dotted curve) calculated from the conductance of E_1. (*b*) Calculation of charge on dots D_1 and D_2, and (*c*) dots D_3 and D_4 during QCA polarization change.

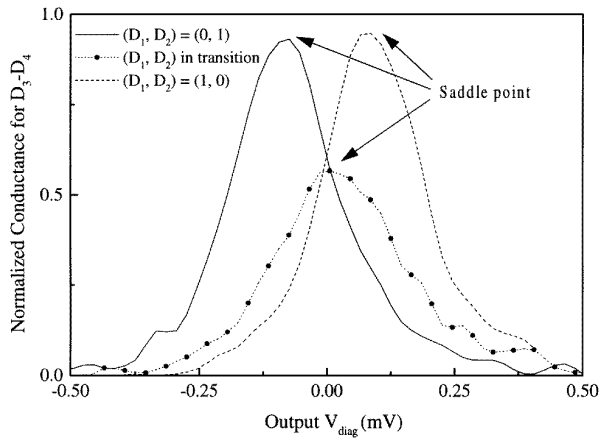

Figure 10. Saddle point conductance lowering for D_3–D_4 during electron switching in D_1–D_2.

4. Estimates of switching frequency

The operation of a large array of QCA cells will depend strongly on the speed at which cells can switch their polarization. Although our experiments were performed at low temperatures using low-noise lock-in amplifiers, we were still able to determine a lower bound for the speed at which switching can occur. We found that the conductance of one double-dot at the cell boundary depended strongly on the charge configuration of the other double-dot. Figure 10 shows the saddle point conductance of the output double-dot for three different charge configurations of the input double-dot. As can be seen in the figure, when the input dots were biased in a stable state, either (1, 0) or (0, 1), so that no current flowed through their series combination, the output double-dots, D_3–D_4, attained the same, high maximum saddle point conductance. However, when the input dots, D_1–D_2, were biased on their saddle point, the peak conductance of the output dots decreased noticeably.

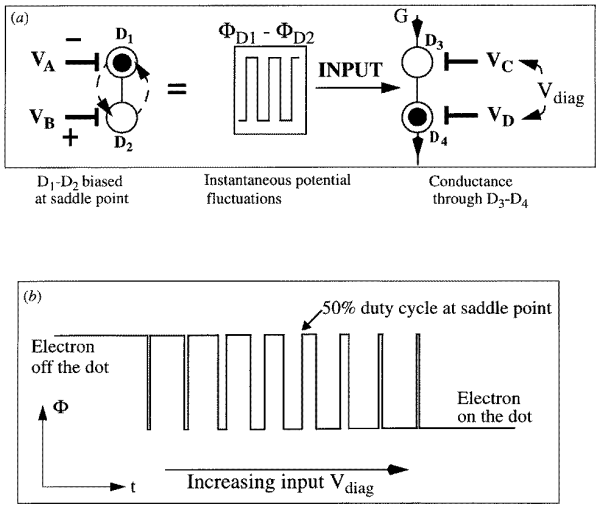

Figure 11. Mechanism for peak lowering of saddle point conductance. (*a*) Electrons effectively hop between D_1 and D_2 resulting in instantaneous potential fluctuations superimposed on the potentials due to the gate voltages V_C and V_D of D_3–D_4 and (*b*) plot of duty cycle of D_1 for increasing input V_{diag}.

We have determined that the mechanism for the peak lowering is the effect of discrete switching events in D_1–D_2 on D_3–D_4. Figure 11 shows the mechanism for the observed peak lowering. For biasing of the dots below the saddle point, in the (1, 0) charged state, electrons tunnel across the junction to D_2, and then off, to be replaced on D_1. This is functionally equivalent to an electron hopping back and forth between D_1 and D_2 resulting in a periodic potential fluctuation, as shown in figure 11(*a*). As the biasing approaches the saddle point, this tunnelling frequency increases, and the duty cycle of the instantaneous potential fluctuations of, e.g., D_1 decreases, approaching 50% for the state where each dot is populated equally, as shown in figure 11(*b*). With further bias into the (0, 1) region on the opposite side of the saddle point, the average population of D_1 decreases with decreased tunnelling frequency, and the duty cycle for potential fluctuations on D_1 approaches zero. As with the push–pull operation of the gate voltages, we are interested in $(\Phi_1^2 - \Phi_2^2)^{1/2}$, related to the difference in potentials between D_1 and D_2, which affects the output dots D_3–D_4 in the same way as V_{diag} in figure 4(*b*). Since the average populations of the dots are equal at the saddle point, the duty cycle for potential fluctuations for each dot is 50% at that bias point.

The effect of the instantaneous voltage fluctuations of the input dots, ΔV_{diag} of figure 11(*a*), is to cause an averaging of the output conductance. Figure 12 is a plot of the output conductance peak across the saddle point versus the output diagonal voltage. The output V_{diag} sets a Q-point on the edge of the conductance peak at the boundary, which is then perturbed by the instantaneous fluctuations. The position of the Q-point, the magnitude of ΔV_{diag}, and its duty cycle (though not the frequency) determine the precise value of the averaging, but under no circumstances can the measured

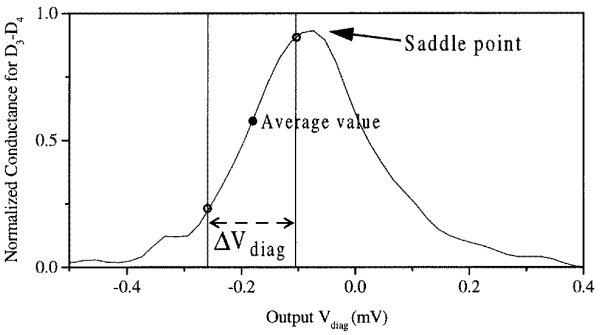

Figure 12. Output conductance peak across the saddle point versus the output diagonal voltage showing averaging due to potential fluctuations of input dots.

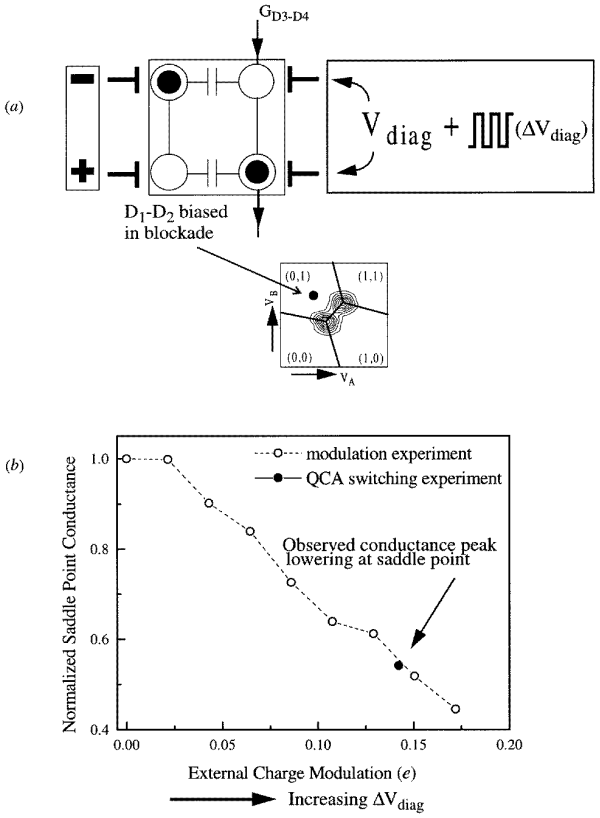

Figure 13. External modulation experiment. (*a*) Schematic diagram of biasing relative to charging diagram and (*b*) normalized saddle point conductance as a function of external charge modulation. The observed output conductance peak lowering at the saddle point is shown as a full circle.

value be as large as the saddle point conductance in the absence of fluctuations.

To test this hypothesis, we performed the experiment described in figure 13(*a*). We biased D_1–D_2 in blockade so as to remove the actual input charge fluctuations, and applied a square wave of 50% duty cycle to the output dots in order to mimic the effect of the input potential fluctuations. We then adjusted the amplitude of the artificial potential fluctuations to achieve the same saddle point lowering as in figure 10. Figure 13(*b*) shows the saddle point lowering of figure 10 superimposed on a plot of the induced conductance peak lowering as a function of the external charge modulation. The external charge modulation is the product of the amplitude of the applied voltage, ΔV_{diag}, and the gate capacitance. We find nearly exact agreement between the peak lowering due to charge modulation on D_3–D_4 by our artificially applied ΔV_{diag} and that due to the input dot charge modulation. Therefore, we conclude that the conductance lowering is due to the instantaneous switching of the input double-dot.

We use an estimate of the frequency of the input fluctuations as a lower bound to the maximum switching frequency of the cell. For our structures, the junction resistance, R_{j}, at low temperature is 1.5 MΩ, and based on a thermally-activated tunnelling rate of $\Gamma = kT/e^2R_{\mathrm{j}}$ we calculate a switching frequency of 14 MHz (since two tunnelling events are required for one switching cycle). The switching frequency would be greater than 50 GHz at room temperature, but would be limited by an *RC* time constant of about 5.5 GHz for a room temperature junction resistance of 750 kΩ and tunnel junction capacitance of 240 aF. The maximum switching speed could be much higher for future devices with optimized designs.

5. Summary and conclusions

We have presented a series of experiments in the metal/tunnel junction system investigating the switching properties of QCA cells. We have shown that the transfer of single electrons between dots can induce opposite switching in an adjacent pair of dots, and that QCA switching operation can be achieved. We concluded that based on these results it is reasonable to anticipate the successful operation of larger arrays of QCA cells. In addition, we determined that instantaneous potential fluctuations of the input dot population led to a low-temperature switching of the output dots at a thermal frequency of 14 MHz. We estimated that a reasonable upper bound for QCA cell switching is likely to be on the order of several GHz, based on RC time constant constraints. This should allow extremely high frequency operation of future QCA systems. Experiments are underway to determine the properties of a cell in which all four dots are coupled by tunnel junctions. Our calculations show that for this system, switching of the input polarization will result in much greater output polarization.

Acknowledgments

This research was supported in part by ARPA, ONR (grant no N0014-95-1-1166) and NSF. The authors wish to thank W Porod and J Merz for helpful discussions.

References

[1] Schaller R R 1997 *IEEE Spectrum* 53–9
[2] Edelstein D *et al* 1997 *Proc. IEEE Int. Electron Devices Meeting* 773–6
Venkatesan S *et al* 1997 *Proc. IEEE Int. Electron Devices Meeting* 769–72
[3] Matsuura M, Tottori I, Goto K, Maekawa K, Mashiko Y and Hirayama M 1997 *Proc. IEEE Int. Electron Devices Meeting* 785–8
[4] Bloomstein T M, Horn M W, Rothschild M, Kunz R R, Palmacci S T and Goodman R B 1997 *J. Vac. Sci. Technol.* B **15** 2112–6

[5] Canning C 1997 *J. Vac. Sci. Technol.* B **15** 2109–11
[6] Lent C S, Tougaw P D, Porod W and Bernstein G H 1993 *Nanotechnology* **4** 49–57
[7] Lent C S, Tougaw P D and Porod W 1993 *Appl. Phys. Lett.* **62** 714–5
[8] Lent C S and Tougaw P D 1997 *Proc. IEEE* **85** 541–57
[9] Tougaw P D and Lent C S W 1994 *J. Appl. Phys.* **75** 1818
[10] Lent C S and Tougaw P D 1994 *J. Appl. Phys.* **75** 4077
[11] Bazán G, Orlov A O, Snider G L and Bernstein G H 1996 *J. Vac. Sci. Technol.* B **14** 4046–50
[12] Orlov A O, Amlani I, Bernstein G H, Lent C S and Snider G L 1997 *Science* **277** 928–30
[13] Snider G L, Orlov A O, Amlani I, Bernstein G H, Lent C S, Merz J L and Porod W 1998 *Semicond. Sci. Technol.* **13** A130
[14] Snider G L, Orlov A O, Amlani I, Bernstein G H, Lent C S, Merz J L and Porod W 1998 *Solid-State Electron.* **42** 1355
[15] Amlani I, Orlov A O, Snider G L, Lent C S and Bernstein G H 1998 *Appl. Phys. Lett.* **72** 2179
[16] Kamins T I and Williams R S 1997 *Appl. Phys. Lett.* **71** 1201–3
[17] Lafarge P, Pothier H, Williams E R, Esteve D, Urbina C and Devoret M H 1991 *Z. Phys.* B **85** 327
[18] Fulton T A and Dolan G H 1987 *Phys. Rev. Lett.* **58** 109
[19] Pothier H, Lafarge P, Urbina C, Esteve D and Devoret M H 1992 *Europhys. Lett.* **17** 249
[20] Meirav U, McEuen P L, Kastner M A, Foxman E B, Kumar A and Wind S J 1991 *Z. Phys.* B **85** 357